A Shape-First, Feed-Next Design Approach for Compact Planar MIMO Antennas

Binbin Yang[1], Juncheng Zhou[2], and Jacob J. Adams[2, *]

Abstract—Employing characteristic mode theory (CMT), a *shape-first feed-next* design methodology for compact planar antennas is proposed, which facilitates rapid and systematic design of self-matched, multi-port antennas with optimal bandwidth and high isolation. First, the optimal antenna shape with multiple self-resonant modes is synthesized using a binary genetic algorithm. Then, the optimal feed positions that provide good input matching and high isolation between the excitation ports are specified using a virtual probe modeling technique. A two-port microstrip antenna with an electrical size of $0.45\lambda_d \times 0.297\lambda_d$ is designed, fabricated and measured. The measured operating frequency is within 1% of the full wave simulation, and the overall S parameter characteristics and far field patterns agree well with the simulation result, validating our design methodology. Mutual coupling $S_{21} < -35\,\text{dB}$ at the center frequency is achieved in this design.

1. INTRODUCTION

Multi-input multi-output (MIMO) communications enable a linear increase in spectral efficiency as the number of transmitting and receiving antennas increases [1], and have been incorporated into many recent wireless standards. However, the design of compact, planar antennas with multiple, decoupled ports remains a challenging problem. Many reported MIMO antenna designs rely on heuristic manipulation of the antenna and ground plane to reduce the mutual coupling effects between the closely spaced antenna elements [2–6]. While these designs can be effective, the lack of a systematic design approach means that little knowledge can be applied to other application scenarios. In [7], a systematic design method for rectangular multimode patch antennas is proposed based on an analytical eigenfunction expansion. A three-port MIMO antenna is demonstrated therein. However, this approach can only be applied to antennas with simple geometry for which the eigenfunctions can be found analytically.

Alternatively, several interesting designs have been reported based on characteristic mode theory (CMT) [8–11], a numerical eigenmode expansion that offers useful properties for MIMO such as orthogonal radiation fields [12]. These methods attempt to design feed schemes that excite the characteristic modes of a predefined antenna aperture (e.g., a rectangular conductor representing a phone chassis) as the characteristic modes are inherently decoupled. While interesting, this approach typically requires external matching and decoupling networks to achieve high return loss and isolation because the modes of the chassis are not resonant at the desired operating frequency in general.

In this paper, we describe a systematic design process to generate self-resonant, planar MIMO antennas without need for external matching or decoupling. This approach is based on the combination of a feed-independent shape synthesis method [13] that generates broadband, self-resonant characteristic modes followed by the rapid assessment of feed positions that excite these modes with minimal coupling.

* Corresponding author: Jacob J. Adams (jjadams2@ncsu.edu).
[1] Motorola Mobility, A Lenovo Company, Chicago, IL, USA. [2] Department of Electrical and Computer Engineering, North Carolina State University, Raleigh, NC, USA.

We call this a *shape-first, feed-next* design strategy for planar MIMO antennas because it separates these two design steps in order to reduce the complexity of the process. The approach is suitable for automated design once the initial constraints have been specified and reduces the need for manual iterative design of the antenna structure.
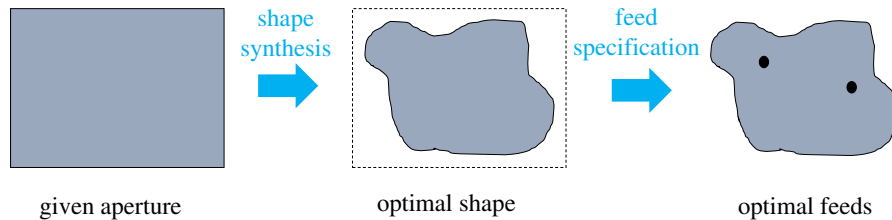
A preliminary investigation of this approach was conducted in [14], where a two port patch antenna over an air substrate was simulated. In the present paper we extend this analysis to antennas on a dielectric substrate by implementing dyadic Green's functions [15] to model the fields within the microstrip substrate and extend model's validity to non-air substrates. For the first time, we present a prototype and measured data for a compact planar MIMO antenna designed using this method. In Section 2, we describe the design methodology and its advantages compared to other approaches. In Section 3, a design example following the proposed methodology is studied and is then verified experimentally in Section 4.

2. SHAPE-FIRST, FEED-NEXT DESIGN METHOD

The characteristic modes represent a set of current patterns supported by the antenna structure, but the specific set of modes present in any real antenna will be determined by the excitation. Still, fundamental properties of the modes, such as resonance frequency, Q factor, and efficiency, can be calculated without knowledge of the feed used to excite them [13, 16]. Thus, we separate the optimization of a planar MIMO antenna design into two independent, sequential steps:

(i) *Find the optimal antenna geometry through feed-independent shape synthesis;*

(ii) *Locate the feed positions on the optimized antenna aperture that achieve acceptable input matching and isolation.*

We call this method a *shape-first, feed-next* design methodology based on the two steps in the process as illustrated in Figure 1. This method can significantly reduce the complexity of planar MIMO antenna design in situations where no canonical design is known. For example, if there are M shapes to be searched for the optimal antenna shape and for each shape there are N potential feed combinations (N increases rapidly with the number of ports [17]), a brute force search will result into $M \times N$ searches. However, by separating the shape and the feed design, only $M + N$ searches are necessary, making the antenna design significantly faster.

Figure 1. Illustration of shape-first, feed-next design methodology.

In the shape synthesis step, the antenna aperture must be designed to support a number of characteristic modes with acceptable properties equal to the number of desired ports. These properties could include fundamental modal properties such as resonance frequency, Q factor, or radiation efficiency. Feed-independent antenna shape synthesis has been reported for single-port antennas [18], and we have recently extended this approach to planar MIMO antennas [13] which we will leverage in this work. Optimizing the aperture based on the modal properties alone enables generation of an aperture that supports the desired modes without the complexity of simultaneously realizing matched and decoupled feeds.

Then in the feed placement step, the optimized antenna geometry is assumed to be probe-fed. The input impedances at all possible feed positions on the optimized aperture are evaluated using an approximate but fast technique, based on a virtual probe concept [17]. The physical feed probes are

represented by current filaments and the modes of the feed-less antenna aperture are used to expand the self- and mutual-impedances of virtual probes placed at any position on the aperture. For small antennas, only a small number of modes are typically needed to accurately model the impedance. This modeling technique facilitates simple feed specification through visualization of the spatial variation of the input parameters as will be demonstrated in the next section.

Both design steps are applicable to planar antennas that are directly fed by a probe. In the shape synthesis step, a variety of optimization constraints can be applied to antenna's properties such as the modal quality factors and modal significance, as well as geometric quantities such as the surface area or maximum dimension occupied by metal. Geometric symmetry can be enforced to reduce the number of optimization variables, but it is not required. The feed placement step is based on a planar antenna circuit model [17] that applies to thin planar antennas above an electrically large plane such that the vertical E field under the patch can be assumed to be uniform, and these models are expected to become less accurate for electrically thick planar antennas.

3. DESIGN EXAMPLE: COMPACT 2.4 GHZ MIMO ANTENNA

In this section, we demonstrate the application of a shape-first, feed-next design process to a compact MIMO antenna design. In this example, a two-port planar MIMO antenna operating at 2.4 GHz is designed. The antenna is placed on a 3.175 mm thick Rogers RT/duroid 5880 ($\epsilon_r = 2.2$) board and is constrained to fit within a rectangular area that is 3.8 cm × 2.5 cm, resulting in an electrical size of $0.45\lambda_d \times 0.297\lambda_d$ at 2.4 GHz. Since a two-port square patch antenna would require lateral dimensions of roughly $0.5\lambda_d \times 0.5\lambda_d$, this rectangular aperture is electrically small and will not be resonant without modification of the aperture.
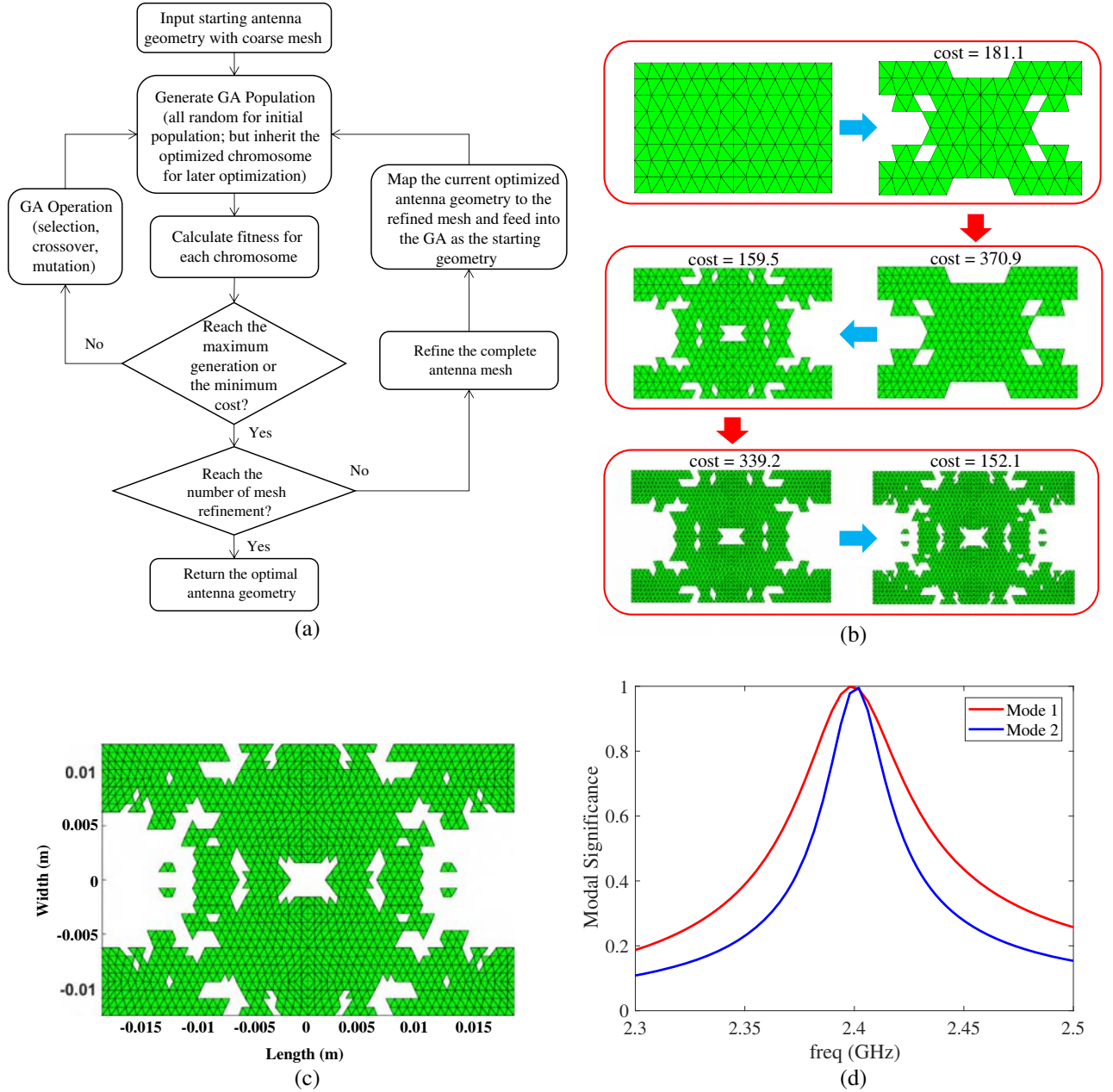
3.1. Step 1: Shape Synthesis

The common approach to this design would be to alter the aperture by adding slots or other features to reduce the resonant frequencies while simultaneously moving the two antenna feeds on the aperture to find high return loss and isolation. In the proposed shape-first, feed-next design method, the first step is the antenna shape synthesis irrespective of any feed considerations. We use a binary genetic algorithm similar to [13] to optimize the fundamental modal parameters by minimizing a cost function. The cost function is defined as

$$\text{cost} = C_1 + C_2 + 10A \tag{1}$$

where $C_n = 200(1 - \text{MS}_n) + Q_n$, and $\text{MS}_n = 1/|1 + j\lambda_n|$ and Q_n are the modal significance and modal Q factor of the n-th mode. A is the normalized area occupied by the conductor and is included to penalize unnecessary conductor "islands". This cost function facilitates the search for an aperture that supports two broadband (low Q factor) and self-resonant characteristic modes. The modal Q factors here are approximated by the frequency derivative of the eigenvalues ($Q_n \approx \frac{f}{2}\frac{d\lambda_n}{df}$). Prior work shows that the modal Q factors generated using this approach can quite closely approach the Q factors of the modes of the entire aperture [13], but these modes are non-resonant in general.

To accelerate the optimization, an adaptive optimization technique is developed, where the antenna optimization begins with a coarse triangular mesh, and once the cost is minimized, the mesh is refined and the optimal geometry from previous iteration is seeded into the next GA optimization [14]. The flowchart that illustrates this adaptive shape synthesis technique is shown in Figure 2(a). Figure 2(b) shows the progression of the antenna shape optimization with two mesh refinement steps. It is worth noting that at each refinement step, the cost changes, which implies that the coarse mesh is not enough to model the antenna resonance behavior. This process can be further repeated with a finer mesh, but we stopped after two meshing refinement steps, considering the increasing computational cost and modest change in the optimized geometry. The final optimized geometry is shown in Figure 2(c). Figure 2(d) shows the modal significance of the first two characteristic modes of the optimized antenna aperture, illustrating that they both resonate at the intended frequency (i.e., MS = 1.), but with different bandwidths, owing to the increasing Q of higher order modes [13].
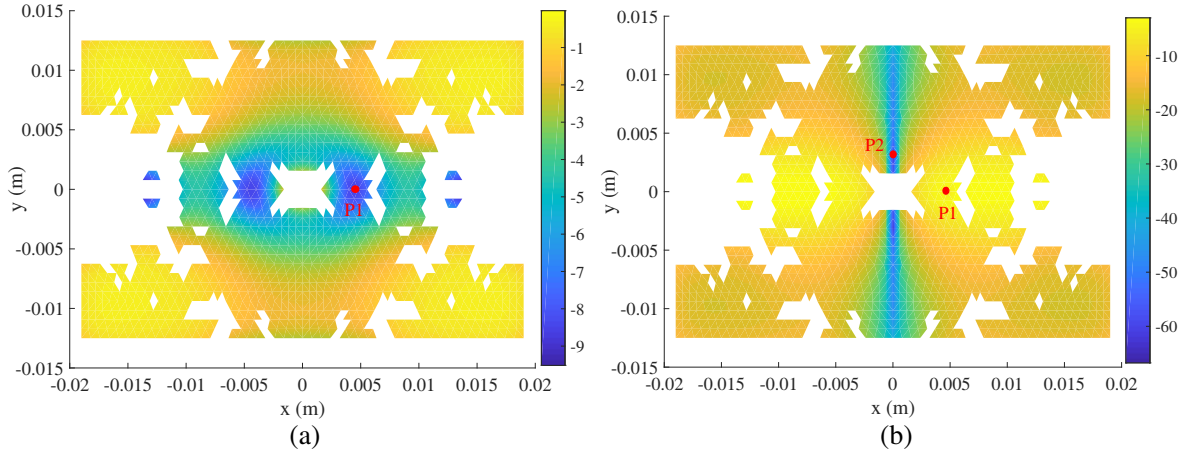
(a)

(b)

(c)

(d)

Figure 2. (a) The algorithm for antenna shape synthesis, (b) the progression of the antenna optimization with two meshing refinement steps, (c) the optimized antenna top metal geometry, and (d) the modal significance of the first two characteristic modes on the optimized antenna.

3.2. Step 2: Feed Specification

Once the optimal antenna aperture is determined through shape synthesis, the next step is to find feed positions that provide acceptable input matching and high isolation on this aperture. Extending prior work on fast modal impedance calculations [17] to antennas over a dielectric substrate[†], we can rapidly estimate the input reflection coefficient of a probe placed at any position in the optimized aperture.

[†] Extension of the results of [17] to planar antennas over a dielectric substrate requires a straightforward modification of the Green's functions used to compute the modes. Also, the DC capacitance used in the circuit model [17] is approximated as $C_{dc} \approx \epsilon_r C_0$, where C_0 is the DC capacitance of the planar antenna without a substrate. Further implementation details can be found in a recent dissertation, B. Yang, *A Modal Approach to Compact MIMO Antenna Design*, North Carolina State University, 2017.

Figure 3. (a) Heat map of $|S_{11}|$ (dB) for the optimized antenna at 2.396 GHz, and (b) heat map of $|S_{21}|$ (dB) for the optimized antenna at 2.396 GHz with the first port being fixed at $P1$ (4.76 mm, 0).

Four characteristic modes and an inductive element representing higher order modes are included in the circuit model to accurately model the self and mutual impedance. Figure 3(a) shows a heat map of the predicted variation of the reflection coefficient across the aperture, with the blue regions representing potential feed positions that result in low reflection coefficient. Using this map as a guide, we select the first feed position at $P1 = (4.76 \text{ mm}, 0)$. Note that the choice of the feed position along the primary axes of the antenna is not necessary (c.f., [14]), and the first feed could be placed at other positions within the blue regions in Figure 3(a).
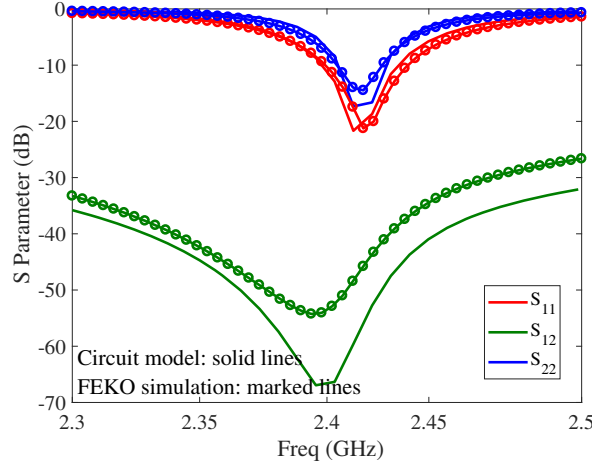
The virtual probe method is then used to predict the coupled impedance at all positions on the aperture given the first port location fixed at $P1$ to generate a heat map of S_{21} values, as shown in Figure 3(b). The blue regions here represent feed positions for port 2 that will result in low mutual coupling with port 1. Combining the S_{11} and S_{21} heat maps in Figure 3, we specify the second feed position at $P2 = (0, 3.108 \text{ mm})$, where both low reflection coefficient and low mutual coupling with respect to port 1 are achieved. Note that the S_{21} heat map will be different if the first feed position $P1$ is selected at a different position (c.f., [14]).

The broadband S-parameters of the two port antenna using the modal circuit model are compared with FEKO simulations that use physical probe feeds in Figure 4. Both self and mutual terms agree closely with the simulation results, showing low reflection coefficient and low mutual coupling in the intended frequency band.
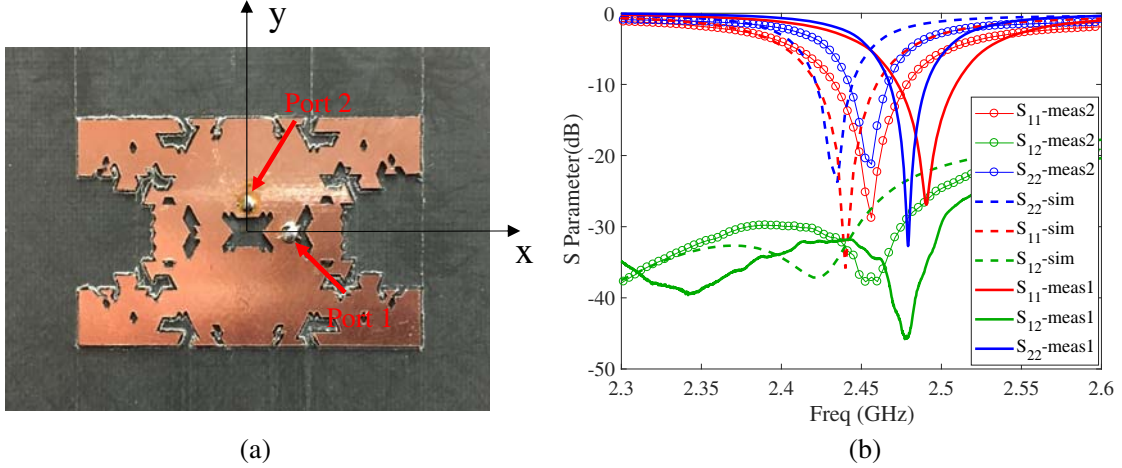
4. FABRICATION AND MEASUREMENT

The method described here is systematic and applicable to a range of geometry and design constraints. However, it relies on CMT for the analysis, which assumes lossless materials, an infinite ground plane and dielectric substrate, and ignores the parasitics of physical RF connectors. We expected that some tuning of the antenna dimensions would be needed once these parameters were accounted for in translation to a real design. Therefore, we conducted simulation in HFSS (Ansys, Inc.), in which a finite substrate, conductor and dielectric losses, and a 3D model of the RF connectors were included. Following these simulation with these physical parameters and parasitics, the antenna geometry was increased in size by 1% in the y dimension to lower the resonant frequency of the second mode, and the feed positions were adjusted by less than 1 mm to $P1' = (4.5 \text{ mm}, 0)$ and $P2' = (0, 2.5 \text{ mm})$ for better input matching. The resulting S-parameters simulated in HFSS are shown as dashed lines in Figure 5(b). The HFSS model shows the same characteristics as the predicted response in Figure 4.

To verify the proposed design, an antenna prototype (Prototype-1) was fabricated on Rogers RT/duroid 5880 using a milling machine and is shown in Figure 5(a). The solid lines in Figure 5(b) show the measured two-port S parameters based on this prototype. The frequency behavior of the fabricated
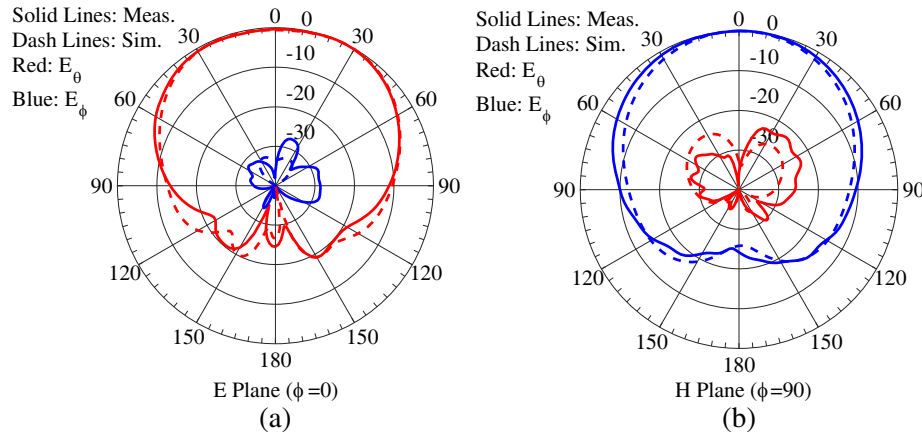
Figure 4. Comparison of the antenna input S parameters from circuit model (solid lines) and full wave simulation (marked lines).

(a)   (b)
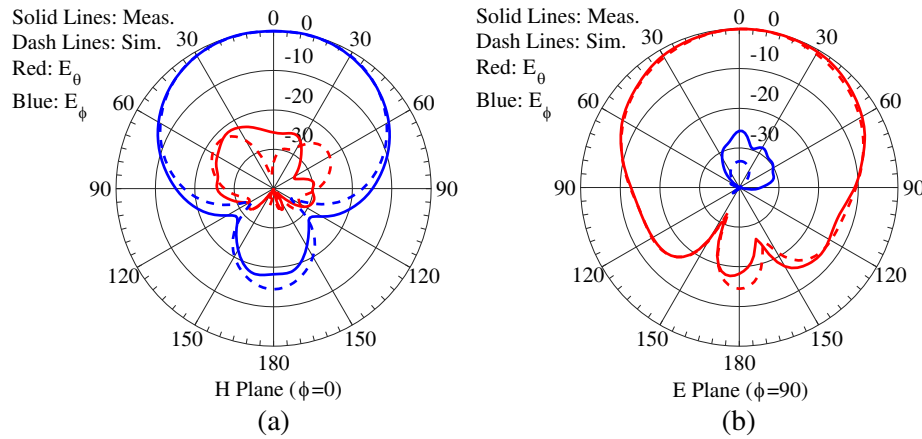
Figure 5. (a) The prototype (Prototype-1) of the 2-port MIMO antenna over microstrip substrate, and (b) the simulation result in HFSS (dashed lines), the measurement result for Prototype-1 (solid lines), and the measurement result for Prototype-2 (marked lines).

antenna shares similar characteristics with simulation results, but the center frequency is offset by about 2%, due to the rough fabrication method. We then fabricated a second prototype (Prototype-2) using a photolithography process, and the measurement data for this prototype is shown as marked lines in Figure 5(b). As expected, with a more accurate fabrication process, the second prototype shows much better agreement with the simulation result (center frequency offset < 1%), verifying the accuracy of our design method. In both cases, all ports are well-matched with extremely low coupling ($S_{21} < -33\,\text{dB}$), despite physical separation of only 5.1 mm.

The 3D far field patterns of Prototype-1 were measured in a Satimo 64 anechoic chamber at the Wireless Research Center of North Carolina. Figures 6 and 7 show the normalized principal pattern cuts of ports 1 and 2 respectively at the respective center frequencies from Figure 5. Close agreement is again observed between the simulation and measurement results. The measured realized gain of port 1 and port 2 at the center frequency of 2.485 GHz are 7.2 dBi and 6.6 dBi respectively, comparing well to the simulated gains of 6.8 dBi and 7.1 dBi at the center frequency of 2.435 GHz. The measured total efficiency of port 1 and port 2 are 91% and 80% respectively at the center frequency. The patterns of the two excited ports are visibly cross-polarized, suggesting some degree of decoupling. In order to

Figure 6. Normalized radiation patterns of port 1: (a) E plane ($\phi = 0$), and (b) H plane ($\phi = 90$); the solid lines are the measurement results at center frequency 2.485 GHz and the dashed lines are the simulation results at center frequency 2.435 GHz.

Figure 7. Normalized radiation patterns of port 2: (a) H plane ($\phi = 0$), and (b) E plane ($\phi = 90$); the solid lines are the measurement results at center frequency 2.485 GHz and the dashed lines are the simulation results at center frequency 2.435 GHz.
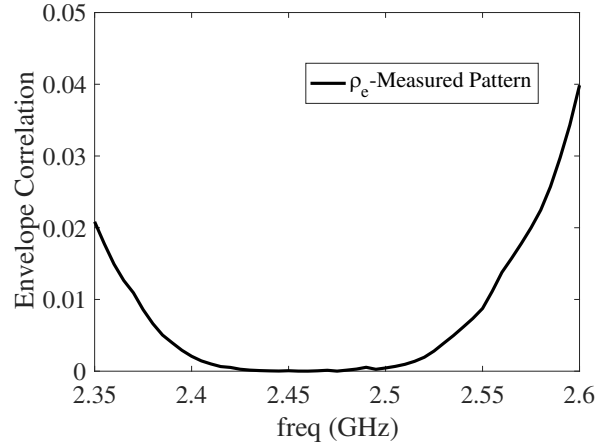
Table 1. Comparison of proposed design with prior art.

Metrics / Designs	−10 dB Bandwidth	Isolation (dB)	Efficiency (%)	Electrical Size
[4] (with parasitic elements)	3.8% (2.52–2.62 GHz)	≥ 20	85	$0.30\lambda_d^2$
[5] (consider first 2 ports)	1.6% (5.15–5.24 GHz)	≥ 20	NA	$0.17\lambda_d^2$
[6] (consider first 2 ports)	2% (2.425–2.475 GHz)	≥ 12	60	$0.27\lambda_d^2$
Proposed Design	1% (2.442–2.467 GHz)	≥ 33	≥ 80	$0.13\lambda_d^2$

precisely characterize the MIMO performance of the antenna, the envelope correlation coefficient (ρ_e) is calculated from the complete set of radiated fields [19] and is shown in Figure 8. Because of the low reflection coefficient and low mutual coupling, the correlation coefficient is very low throughout the band of interest.

In Table 1, we compare the proposed design with other similar work in literature. Bearing in mind that bandwidth scales roughly as the cube of electrical size, the smaller bandwidth of our more

Figure 8. The envelope correlation coefficient calculated from the measured 3D radiation pattern.

compact design is expected. Despite the small aperture, our design is well-matched with high efficiency and excellent isolation. Most importantly, however, this design would never have been identified by a more heuristic process as it is not based on a canonical antenna element (e.g., monopole, slot). The proposed systematic approach can be automated and applied to a variety of design scenarios with differing constraints.

5. CONCLUSIONS

A *shape-first feed-next* design methodology is proposed for planar MIMO antennas. The optimal antenna aperture is synthesized first through a binary genetic algorithm, and then the optimal probe feed positions are selected using fast impedance calculations. Two antenna prototypes are designed and fabricated exhibiting low reflection coefficient and extremely low mutual coupling ($S_{21} < -35\,\text{dB}$) at the center frequency, verifying our proposed design methodology. The proposed method is flexible and can be readily applied to the design of planar MIMO antennas under a variety of geometric and performance constraints. Though other optimization techniques for MIMO antennas have been proposed [20–22], these other methods must assume an initial antenna shape or feed position. The systematic design process described here does not make these assumptions and so provides many more degrees of freedom in both antenna shape and feed placement while reducing the time that would normally be required for a direct search of the design space by dividing the optimization into two sequential steps.

ACKNOWLEDGMENT

REFERENCES

1. Foschini, G. J. and M. J. Gans, "On limits of wireless communications in a fading environment when using multiple antennas," *Wireless Personal Communications*, Vol. 6, No. 3, 311–335, 1998.
2. Liu, L., S. Cheung, and T. Yuk, "Compact MIMO antenna for portable devices in UWB applications," *IEEE Trans. Antennas Propag.*, Vol. 61, No. 8, 4257–4264, 2013.
3. Ren, J., W. Hu, Y. Yin, and R. Fan, "Compact printed MIMO antenna for UWB applications," *IEEE Antennas Wirel. Propag. Lett.*, Vol. 13, 1517–1520, 2014.
4. Soltani, S. and R. D. Murch, "A compact planar printed mimo antenna design," *IEEE Trans. Antennas Propag.*, Vol. 63, No. 3, 1140–1149, 2015.

5. Sarrazin, J., Y. Mahe, S. Avrillon, and S. Toutain, "Collocated microstrip antennas for MIMO systems with a low mutual coupling using mode confinement," *IEEE Trans. Antennas Propag.*, Vol. 58, No. 2, 589–592, Feb. 2010.

6. Soltani, S., P. Lotfi, and R. D. Murch, "A dual-band multiport mimo slot antenna for WLAN applications," *IEEE Antennas and Wireless Propagation Letters*, Vol. 16, 529–532, 2017.

7. Redondo, C. and L. de Haro, "On the analysis and design of reconfigurable multimode MIMO microstrip antennas," *IEEE Trans. Antennas Propag.*, Vol. 62, No. 1, 119–129, 2014.

8. Li, H., Z. T. Miers, and B. K. Lau, "Design of orthogonal MIMO handset antennas based on characteristic mode manipulation at frequency bands below 1 GHz," *IEEE Trans. Antennas Propag.*, Vol. 62, No. 5, 2756–2766, May 2014.

9. Martens, R. and D. Manteuffel, "Systematic design method of a mobile multiple antenna system using the theory of characteristic modes," *IET Microwaves, Antennas & Propagation*, Vol. 8, No. 12, 887–893, 2014.

10. Deng, C., Z. Feng, and S. V. Hum, "MIMO mobile handset antenna merging characteristic modes for increased bandwidth," *IEEE Trans. Antennas Propag.*, Vol. 64, No. 7, 2660–2667, Jul. 2016.

11. Zhang, Q., R. Ma, W. Su, and Y. Gao, "Design of a multimode UWB antenna using characteristic mode analysis," *IEEE Trans. Antennas Propag.*, Vol. 66, No. 7, 3712–3717, Jul. 2018.

12. Harrington, R. and J. Mautz, "Theory of characteristic modes for conducting bodies," *IEEE Trans. Antennas Propag.*, Vol. 19, No. 5, 622–628, 1971.

13. Yang, B. and J. J. Adams, "Systematic shape optimization of symmetric MIMO antennas using characteristic modes," *IEEE Trans. Antennas Propag.*, Vol. 64, No. 7, 2668–2678, 2016.

14. Yang, B. and J. J. Adams, "A modal approach to shape synthesis and feed placement for planar MIMO antennas," *Proc. 2016 IEEE Int. Symp. Antennas and Propagation*, 15–16, 2016.

15. Chow, Y. L., J. Yang, D. Fang, and G. Howard, "A closed-form spatial Green's function for the thick microstrip substrate," *IEEE Transactions on Microwave Theory and Techniques*, Vol. 39, No. 3, 588–592, 1991.

16. Capek, M., J. Eichler, and P. Hazdra, "Evaluating radiation efficiency from characteristic currents," *IET Microwaves, Antennas & Propagation*, Vol. 9, No. 1, 10–15, 2014.

17. Yang, B. and J. J. Adams, "Computing and visualizing the input parameters of arbitrary planar antennas via eigenfunctions," *IEEE Trans. Antennas Propag.*, Vol. 64, No. 7, 2707–2718, Jul. 2016.

18. Ethier, J. L. and D. A. McNamara, "Antenna shape synthesis without prior specification of the feedpoint locations," *IEEE Trans. Antennas Propag.*, Vol. 62, No. 10, 4919–4934, 2014.

19. Blanch, S., J. Romeu, and I. Corbella, "Exact representation of antenna system diversity performance from input parameter description," *Electronics Lett.*, Vol. 39, No. 9, 705–707, 2003.

20. Soltani, S., P. Lotfi, and R. D. Murch, "Design and optimization of multiport pixel antennas," *IEEE Trans. Antennas Propag.*, Vol. 66, No. 4, 2049–2054, Apr. 2018.

21. Lu, D., L. Wang, E. Yang, and G. Wang, "Design of high-isolation wideband dual-polarized compact MIMO antennas with multiobjective optimization," *IEEE Trans. Antennas Propag.*, Vol. 66, No. 3, 1522–1527, Mar. 2018.

22. Mallahzadeh, A. R., S. Es'haghi, and A. Alipour, "Design of an E-shaped MIMO antenna using iwo algorithm for wireless application at 5.8 GHz," *Progress In Electromagnetics Research*, Vol. 90, 187–203, 2009.